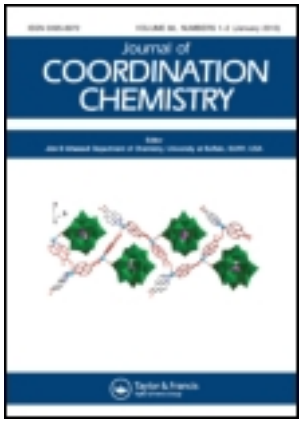

Journal of Coordination Chemistry
Publication details, including instructions for authors and subscription information:
http://www.tandfonline.com/loi/gcoo20

Ruthenium(II/IV) complexes with potentially tridentate Schiff base chelates containing the uracil moiety

Irvin Noel Booysen[a], Sanam Maikoo[a], Matthew Piers Akerman[a], Bheki Xulu[a] & Orde Munro[a]

[a] School of Chemistry and Physics, University of Kwazulu-Natal, Pietermaritzburg, South Africa

Accepted author version posted online: 04 Oct 2013.Published online: 06 Nov 2013.

To cite this article: Irvin Noel Booysen, Sanam Maikoo, Matthew Piers Akerman, Bheki Xulu & Orde Munro (2013) Ruthenium(II/IV) complexes with potentially tridentate Schiff base chelates containing the uracil moiety, Journal of Coordination Chemistry, 66:20, 3673-3685, DOI: 10.1080/00958972.2013.849808

To link to this article: http://dx.doi.org/10.1080/00958972.2013.849808

Journal of Coordination Chemistry, 2013
Vol. 66, No. 20, 3673–3685, http://dx.doi.org/10.1080/00958972.2013.849808

Ruthenium(II/IV) complexes with potentially tridentate Schiff base chelates containing the uracil moiety

IRVIN NOEL BOOYSEN*, SANAM MAIKOO, MATTHEW PIERS AKERMAN, BHEKI XULU and ORDE MUNRO

School of Chemistry and Physics, University of Kwazulu-Natal, Pietermaritzburg, South Africa

(*Received 25 June 2013; accepted 28 August 2013*)

Herein we report the synthesis and characterization of *trans*-[$Ru^{II}Cl_2(PPh_3)_3$] with potentially tridentate Schiff bases derived from 5,6-diamino-1,3-dimethyl uracil (H_2ddd) and two 2-substituted aromatic aldehydes. In the diamagnetic ruthenium(II) complexes, *trans*-[$RuCl(PPh_3)_2$(Htdp)] (**1**) {H_2tdp = 5-((thiophen-3-*yl*)methyleneamino)-6-amino-1,3-dimethyluracil} and *trans*-[RuCl(PPh_3)$_2$(Hsdp)] (**2**) {H_2sdp = 5-(2-(methylthio)benzylideneamino)-6-amino-1,3-dimethyluracil}, the Schiff base ligands (i.e. Htdp and Hsdp) act as mono-anionic tridentate chelators. Upon reacting 5-(2-hydroxybenzylideneamino)-6-amino-1,3-dimethyluracil (H_3hdp) with the metal precursor, the paramagnetic complex, *trans*-[$Ru^{IV}Cl_2$(ddd)(PPh_3)$_2$] (**3**), was isolated, in which the bidentate dianionic ddd co-ligand was formed by hydrolysis. The metal complexes were fully characterized via multinuclear NMR-, IR-, and UV–Vis spectroscopy, single crystal XRD analysis and conductivity measurements. The redox properties were probed via cyclic voltammetry with all complexes exhibiting comparable electrochemical behavior with half-wave potentials ($E_{½}$) at 0.70 V (for **1**), 0.725 V (for **2**), and 0.68 V (for **3**) *versus* Ag|AgCl, respectively. The presence of the paramagnetic metal center for **3** was confirmed by ESR spectroscopy.

Keywords: Ruthenium(II/IV); Schiff base; Uracil; Crystal structure; Spectral characterization

1. Introduction

Ruthenium Schiff base complexes have been extensively investigated for their potential therapeutic applications for various diseases due to their potent antiviral, antibacterial, and antimicrobial activities [1–4]. These complexes have increased activities with respect to their free Schiff bases, where the activity is typically enhanced upon coordination [5]. Schiff bases commonly stabilize the low-spin diamagnetic d^6 ruthenium(II) metal center through chelation and multidenticity [6]. Donor manipulation of Schiff bases affords stabilization of higher oxidation states of ruthenium. For example, a series of paramagnetic ruthenium(III) Schiff base complexes, *trans*-[$Ru^{III}Cl(L)(PPh_3)_2$] was isolated from the respective coordination reactions between *trans*-[$Ru^{II}Cl_2(PPh_3)_2$] and Schiff bases (*L*) derived from various acid hydrazides and benzaldehyde [7]. Recently, the nitrido metal complex *trans*-[Ru^{VI}(N)(H_2O)(imp)$_2$][OTf] (OTf^- = triflate) was reported, in which the 2-[(2,6-diisopropylphenyl)imino]methyl-4,6-dibromophenolate (imp^-) chelators coordinate in a bidentate manner through singly deprotonated phenolic oxygens and neutral imino nitrogens [8].

*Corresponding author. Email: Booyseni@ukzn.ac.za

Currently, the first ruthenium chemotherapeutic drug, NAMI-A, (ImH)[*trans*-$RuCl_4(DMSO)(Im)$] {Im = imidazole} has recently entered Phase II clinical trials due to its optimal antimetastatic cancer activity accompanied with fewer significant side effects than platinum-based metallopharmaceuticals [9]. Further development of this class of ruthenium complexes depends on attachment of biological moieties which can manipulate the biodistribution [10]. Particular interest to us is 5,6-diamino-1,3-dimethyl uracil (H_2ddd) which is an analog of the established chemotherapeutic drug, uracil mustard [11]. We have previously shown that Schiff base derivatives of H_2ddd have diverse coordination modes toward rhenium in both high and low oxidation states [12, 13], as in the case of reaction between *cis*-$[Re^{V}O_2I(PPh_3)_2]$ and H_3hdp [*N*-(2-hydroxybenzylidene)-5-amino-1,3-dimethyluracil] which led to the imido compound, *trans*-$[Re^{V}$(ddd)(Hduo)$(PPh_3)_2]I$ [12]. Furthermore, the rhenium(I) complex *fac*-$[Re^{I}(CO)_3Br(adp)]$ was isolated from the equimolar reaction between 5-amino-1,3-dimethyl-6-(pyridin-2-*yl*-methylidene)uracil (adp) and $[Re(CO)_5Br]$ [13]. Ruthenium compounds with derivatives of uracil and other nucleotide bases are known, e.g. the ruthenium(III) compounds, $[RuCl_4(DMSO)[H\text{-}L^{A})]]$ {L^{A} = N^6-pentyladenine, N^6-hexyladenine or N^6,N^6-dibutyladenine} [14–16].

In this study, the coordination of various Schiff bases synthesized from a derivative of the biologically relevant moiety, uracil [*viz*. 5,6-diamino-1,3-dimethyl uracil (H_2ddd)], toward ruthenium(II) are explored. The ruthenium complexes *trans*-$[Ru^{II}Cl(PPh_3)_2$(Htdp)] (**1**) and *trans*-$[Ru^{II}Cl(PPh_3)_2$(Hsdp)] (**2**) were isolated from reactions with the Schiff bases 5-((thiophen-3-*yl*)methyleneamino)-6-amino-1,3-dimethyluracil (H_2tdp) and 5-(2-(methylthio)benzylideneamino)-6-amino-1,3-dimethyluracil (H_2sdp), respectively. Schiff base hydrolysis occurs upon reacting 5-(2-hydroxybenzylideneamino)-6-amino-1,3-dimethyluracil (H_3hdp) which led to a paramagnetic ruthenium(IV) complex, *trans*-$[Ru^{IV}Cl_2$(ddd)$(PPh_3)_2]$ (**3**).

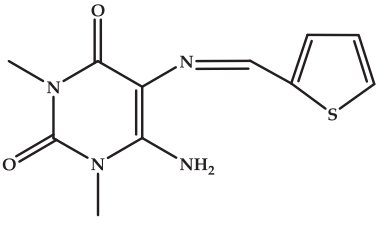

H_2tdp

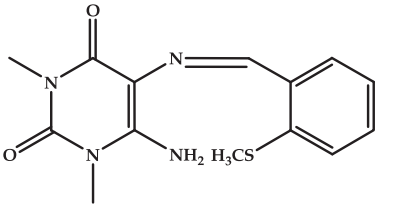

H_2sdp

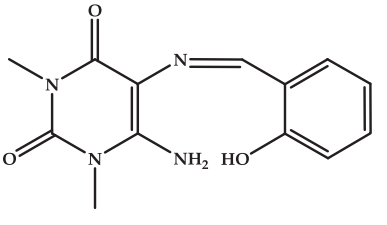

H_3hdp

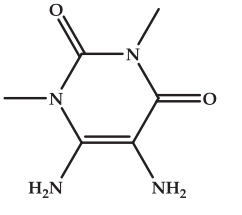

H_2ddd

2. Experimental

2.1. *Materials and methods*

Trans-$[RuCl_2(PPh_3)_3]$, salicylaldehyde, thiophene-2-carbaldehyde, 2-methylthiobenzaldehyde and 5,6-diamino-1,3-dimethyluracil were obtained from Sigma–Aldrich. All solvents

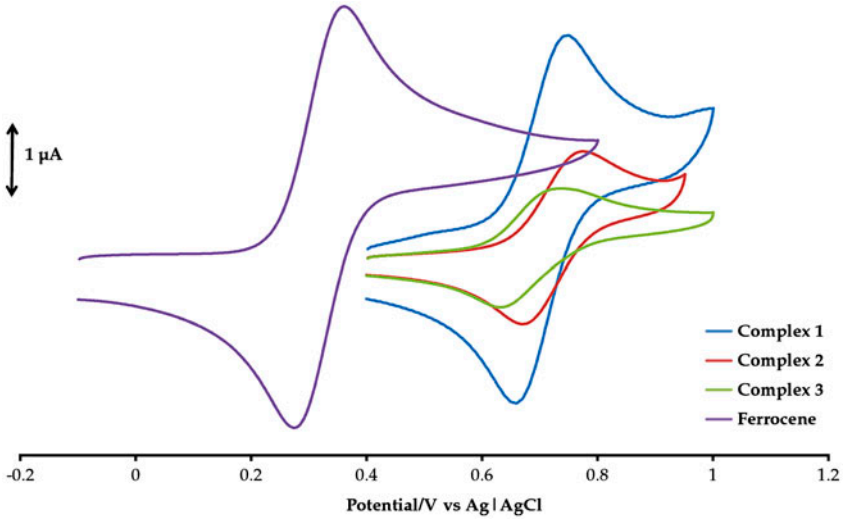

Figure 1. Overlay cyclic voltammograms of **1**, **2** and **3** as well as for the ferrocene standard. The potential windows for the complexes are between 0.4 and 1 V while for ferrocene between −0.1 and 0.8 V. All experiments were done at a scan rate of 100 mV s^{-1}.

were obtained from Merck SA. The chemicals were used without purification. The Schiff bases, H_3hdp and H_2sdp, were synthesized as previously reported from the condensation reactions between H_2ddd and 2-methylthiobenzaldehyde, and salicylaldehyde, respectively [12, 17]. Ultrapure water was produced from an Elga Purelab Ultra system.

Infrared spectra were recorded on a Perkin-Elmer Spectrum 100 from 4000 to 650 cm^{-1}. The ^{1}H and ^{31}P NMR spectra were obtained using a Bruker Avance 400 MHz spectrometer. UV–Vis spectra were recorded using a Perkin Elmer Lambda 25. The extinction coefficients (ε) are given in dm^3 M^{-1} cm^{-1}. The X-band EPR spectrum was obtained from a Bruker EMX Premium X spectrometer. Melting points were determined using a Stuart SMP3 melting point apparatus. Conductivity measurements were determined at 295 K on a Radiometer R21M127 CDM 230 conductivity and pH meter.

Cyclic voltammetry measurements were done using an Autolab potentiostat equipped with a three electrode system, a glassy carbon working electrode (GCWE), a pseudo Ag|AgCl reference electrode, and an auxiliary Pt counter electrode. The Autolab Nova 1.7 software was utilized for operating the potentiostat and data analysis. The ruthenium complexes were made up in 2 mM solutions in DCM along with tetrabutylammonium hexafluorophosphate (0.1 M) as a supporting electrolyte. Between each measurement, the GCWE electrode surface was polished with slurry of ultrapure water and alumina on a Buehler felt pad, which was followed by rinsing with excess ultrapure water and ultra-sonication in absolute ethanol. Ferrocene was used as a standard and its cyclic voltammogram is shown in figure 1.

2.2. *Synthesis of 5-((thiophen-3-yl)methyleneamino)-6-amino-1,3-dimethyluracil (H_2tdp)*

H_2ddd (0.500 g; 2.94 mM) and thiophene-2-aldehyde (0.399 mL; 4.41 mM) were refluxed for 3 h in methanol (40 cm^3). The resulting dark yellow solution was allowed

to cool to room temperature, filtered, and a bright yellow precipitate was washed with cold anhydrous toluene as well as diethyl ether. Yield = 63%; m.p. 182.7–184.5°C. IR (ν_{max} cm^{-1}): ν(N–H) 3396, 3286 ν(C=O) 1671, ν(C=N) 1611, ν(thiophene) 1506, 1447 and 1380. ^{1}H NMR (295 K/d^6-DMSO ppm^{-1}): 9.79 (s, 1H, H1), 7.58 (d, 1H, H4), 7.41 (d, 1H, H2), 7.95 (t, 1H, H3), 6.96 (br, s, 2H, NH_2), 3.42 (s, 3H, CH_3), 3.18 (s, 3H, CH_3). UV–Vis (DMF, λ_{max} (ε, M^{-1} cm^{-1})): 288 nm (1437), 292 nm (2421), sh, 390 nm (1897).

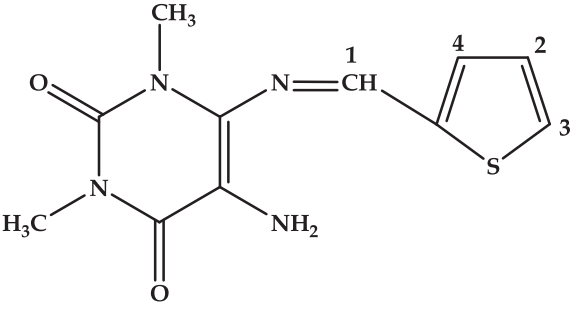

2.3. *Synthesis of trans-[RuCl(PPh$_3$)$_2$(Htdp)] (1)*

H_2tdp (0.0276 g; 0.104 mM) and *trans*-[$RuCl_2(PPh_3)_3$] (0.100 g; 0.104 mM) were refluxed for 3 h in methanol (20 cm^3). While the brick-red solution was allowed to cool to room temperature, red crystals grew in the mother liquor, and were filtered and washed with anhydrous diethyl ether. These crystals were dissolved in dichloromethane and layered with hexane. The slow diffusion of hexane into DCM solution afforded cubic-shaped crystals suitable for X-ray analysis. Yield = 52% based on Ru; m.p. 240.7–242.4°C. Molar conductivity (DCM, 10^{-3} M) = 3.003 Ohm cm^2 M^{-1}. IR (ν_{max} cm^{-1}): ν(N–H) br, 3182, ν(C=O) 1711, ν(C=N) 1665, ν(C=C) 1576, ν(thiophene) 1456, 1436 and 1368, ν(Ru-[PPh_3]$_2$) 746 and 696. ^{1}H NMR (295 K/d^3-CD_3CN ppm^{-1}): 12.72 (s, 1H, NH), 7.71–7.62 (m, 4H, H1, H2, H3, H4), 7.51–7.29 (m, 30H, 2x PPh_3), 3.03 (s, 3H, CH_3), 2.78 (s, 3H, CH_3). ^{31}P NMR (295 K/d^3-CD_3CN ppm^{-1}): 15.28. UV–Vis (DCM, λ_{max} (ε, M^{-1} cm^{-1})): 284 nm (32,864), 406 nm (2265), 507 nm (9385).

2.4. *Synthesis of trans-[RuCl(PPh$_3$)$_2$(Hsdp)] (2)*

Equimolar amounts of H_2sdp (0.0318 g; 0.104 mM) and *trans*-[$RuCl_2(PPh_3)_3$] (0.100 g; 0.104 mM) were refluxed for 3 h in methanol (20 cm^3). The resultant cherry-red solution was allowed to cool to room temperature, and the red crystals were filtered by gravity. The crystals were recrystallized via slow diffusion in a chloroform and hexane (1 : 1) solution. Yield = 61% based on Ru; m.p. 208.4–210.2°C. Molar conductivity (DCM, 10^{-3} M) = 10.31 Ohm cm^2 M^{-1}; IR (ν_{max} cm^{-1}): ν(N–H) br, 3398, ν(S–CH_3) 3066 ν(C=O) sh, 1705, ν(C=N) 1671, ν(C=C) 1577, ν(Ru-[PPh_3]$_2$) 743 and 695. ^{1}H NMR (295 K/d^3-CD_3CN ppm^{-1}): 12.67 (s, 1H, NH), 8.01 (br, s, 1H, H1), 7.75–7.52 (m, 4H, H2, H3, H4, H5), 7.51–7.16 (m, 30H, 2x PPh_3), 6.90 (br, s, 3H, SCH_3), 3.04 (s, 3H, CH_3), 2.77 (s, 3H, CH_3). ^{31}P NMR (295 K/d^3-CD_3CN ppm^{-1}): 24.61. UV–Vis (DCM, λ_{max} (ε, M^{-1} cm^{-1})): 283 nm (7649), 393 nm (1066), 509 nm (1520).

2.5. *Synthesis of cis-Cl, trans-P-[RuCl$_2$(PPh$_3$)$_2$(ddd)] (3)*

A 1 : 1 M reaction of H_3hdp (0.029 g; 0.104 mM) and *trans*-[$RuCl_2(PPh_3)_3$] (0.100 g; 0.104 mM) were refluxed for 3 h in methanol (20 cm^3). The dark maroon solution was allowed to cool to room temperature, dark red crystals were filtered and washed with anhydrous diethyl ether. These crystals which formed were dissolved in dichloromethane and layered with hexane and then the resultant solution was allowed to stand for several days. From slow diffusion of hexane into the DCM solution, XRD quality red crystalline parallelograms were afforded. Yield = 62% based on Ru; m.p. 207.9–209.0 °C. Conductivity (DCM, 10^{-3} M) = 9.433 Ohm cm^2 M^{-1}. IR (ν_{max} cm^{-1}): ν(N–H) 3052, 3148, ν(C=O) 1712, ν(C=C) 1579, ν(Ru-[PPh_3]$_2$) 743 and 697. UV–Vis (DCM, λ_{max} (ε, M^{-1} cm^{-1})): 281 nm (2800), 336 nm (776), 354 nm (619), 372 nm (549), 406 nm (332), 515 nm (690).

2.6. *X-ray diffraction*

X-ray diffraction data were recorded on an Oxford Diffraction Xcalibur 2 CCD 4-circle diffractometer equipped with an Oxford Instruments Cryojet operating at 120(2) K in the case of **1**. The X-ray data for **3** were recorded on a Bruker Apex Duo equipped with an Oxford Instruments Cryojet operating at 100(2) K and an Incoatec microsource operating at 30 W power. Crystal and structure refinement data are given in table 1. Selected bond lengths and angles are given in table 2. In both the cases data were collected with Mo Kα (λ = 0.71073 Å) radiation at a crystal-to-detector distance of 50 mm. The data collection on

Table 1. Crystal data and structure refinement data.

	1	**3·CHCl$_3$**
Chemical formula	$C_{47}H_{41}ClN_4P_2RuS$	$C_{42}H_{38}Cl_2N_4O_2P_2Ru.CHCl_3$
Formula weight	924.36	984.1
Temperature (K)	120(2)	100(2)
Crystal system	*P2$_1$/n*	*P-1*
Space group	Monoclinic	Triclinic
Unit cell dimensions (Å, °)	*a* = 15.0390(50)	*a* = 12.5444(6)
	b = 17.3710(50)	*b* = 12.9786(7)
	c = 16.0210(50)	*c* = 14.9529(8)
	α = 90.000(5)	α = 71.528(3)
	β = 105.876(5)	β = 72.450(3)
	γ = 90.000(5)	γ = 71.853(2)
Crystal size (mm)	0.20 × 0.10 × 0.10	0.4 × 0.05 × 0.05
V (Å^3)	4026(2)	2137.89(19)
Z	4	2
Density (Calcd) (Mg/m^3)	1.525	1.53
Absorption coefficient (mm^{-1})	0.634	0.796
F (000)	1896	1000
θ Range for data collection (°)	2.87–26.06	1.5–27.0
Index ranges	$-18 \le h \le 17$	$-15 \le h \le 15$
	$-21 \le k < 20$	$-16 \le k < 16$
	$-19 \le l \le 19$	$-16 \le l \le 18$
Reflections measured	29,767	25,651
Observed reflections [$I > 2\sigma(I)$]	5483	6780
Independent reflections	7957	7696
Data/restraints/parameters	7957/0/529	7696/2/524
Goodness of fit on F^2	0.862	1.003
Observed *R*, wR^2	0.0360, 0.0756	0.033, 0.083
R_{int}	0.0697	0.021

Table 2. Selected bond lengths [Å] and angles [°] for **1** and **3**.

1		**3**	
Ru–N1	2.036(3)	Ru–N1	2.017(3)
Ru–N2	2.053(2)	Ru–N2	1.969(3)
Ru–Cl	2.4517(9)	Ru–Cl1	2.4218(7)
Ru–P1	2.395(1)	Ru–Cl2	2.4361(8)
Ru–P2	2.372(1)	Ru–P1	2.3878(7)
Ru–S	2.362(1)	Ru–P2	2.4006(7)
C5–N2	1.313(4)	N1–Ru–N2	78.0(1)
C1–S	1.725(3)	Cl1–Ru–Cl2	97.64(2)
C4–S	1.749(3)	Cl1–Ru–N1	175.29(8)
C1–C2	1.353(4)	Cl2–Ru–N2	164.70(7)
C2–C3	1.426(4)	P1–Ru–P2	170.34(2)
C3–C4	1.362(5)	–	–
S–Ru–N2	80.9(7)	–	–
N1–Ru–N2	78.8(1)	–	
Cl–Ru–N2	167.66(7)	–	–
S–Ru–N1	159.14(8)	–	–
C6–N2–C6	123.5(3)	–	
P1–Ru–P2	175.28(3)	–	–

the Oxford diffractometer was performed using omega scans at $\theta = 29.389°$ with exposures taken at 2.00 kW X-ray power and 0.75° frame widths using CrysAlis CCD [18]. The data were reduced with CrysAlis RED Version 170 [18] using outlier rejection, scan speed scaling, as well as standard Lorentz and polarization correction factors. A semi-empirical multi-scan absorption correction [19] was applied to the data. The following conditions were used for the Bruker data collection: Ω and ϕ scans with exposures taken at 30 W X-ray power and 0.50° frame widths using APEX2 [20]. The data were reduced with SAINT [20] using outlier rejection, scan speed scaling, as well as standard Lorentz and polarization correction factors. A SADABS semi-empirical multi-scan absorption correction [20] was applied to the data. Direct methods, SHELXS-97 [21], and WinGX [22] were used to solve all three structures. All non-hydrogen atoms were located in the difference density map and refined anisotropically with SHELXL-97 [21]. All hydrogens of **1** were included as idealized contributors in the least-squares process, but for **3** OLEX 2 was utilized where the hydrogens were treated by a mixture of independent and constrained refinement [23].

3. Results and discussion

3.1. *Synthesis and spectral characterization*

Equimolar reactions between *trans*-[$Ru^{II}Cl_2(PPh_3)_2$] with H_2tdp, H_2sdp, and H_3hdp led to variable valence ruthenium(II/IV) complexes, *trans*-[$Ru^{II}Cl(PPh_3)_2$(Htdp)] (**1**), *trans*-[$Ru^{II}Cl(PPh_3)_2$(Hsdp)] (**2**) and *cis-Cl*, and *trans-P*-[$Ru^{IV}Cl_2(PPh_3)_2$(ddd)] (**3**), in moderate yields, respectively. In **1** and **2**, the Schiff base chelators (i.e. Htdp for **1** and Hsdp for **2**) coordinate as mono-anionic tridentate chelators whereas in **3**, the initial Schiff base (H_3hdp) hydrolyzed to afford the ddd chelator which is a bidentate dianionic moiety. In preparation of **3**, no precaution was taken to ensure that the reaction was performed with a dry solvent and in an inert atmosphere which led to the hydrolysis of H_3dhp to form ddd. The resulting ddd ligand induced oxidation of the metal center upon coordination.

The respective chelators for all the three complexes occupy the equatorial plane with Htdp and Hsdp NNS donors, leaving one remaining position for chloride while ddd affords a five-membered chelator ring through its NN-donor set *trans* to the *cis* chlorides. The bulky PPh_3 ligands are *trans* minimizing steric repulsion. This orientation is typical for ruthenium Schiff base complexes containing $[Ru(PPh_3)_2]$, e.g. *trans*-[Ru(*R*cb)CO(Cl)$(PPh_3)_2$] {H*R*cb = *N*-[dialkyl/aryl)carbamothioyl]benzamide, *R* = alkyl or aryl] [24]. In an attempt to isolate octahedral saturated ruthenium complexes (i.e. "3 + 3" coordination modes), by utilizing higher molar ratios of the respective ligands with respect to the metal precursor, the same metal complexes (i.e. **1**, **2** and **3**) were isolated. Recently, the "3 + 3" ruthenium(III) compounds, $[Ru(L^n)_2]ClO_4$ {(HL^n = 4-*R*-2-((2-(pyridin-2-*yl*)hydrazono) methyl)phenol, *R* = H, Cl, Br, Me, and OMe}, have been reported [6, 25].

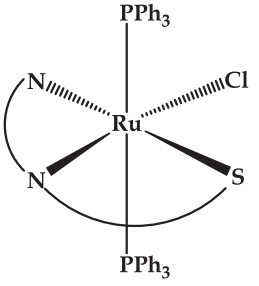

1

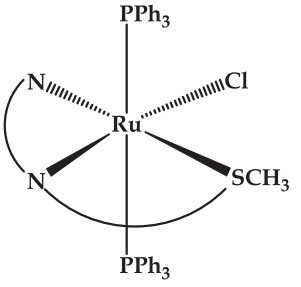

2

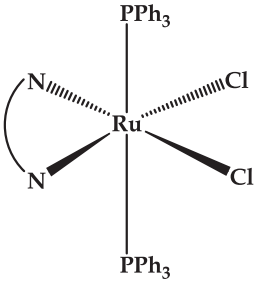

3

The Schiff bases were only soluble in DMF and DMSO, but the complexes exhibit good solubility in most polar solvents and are non-electrolytes in DCM. NMR spectroscopy for the ligands (in d^6-DMSO) and complexes (d^3-CD_3CN) was done in different deuterated solvents, since no interpretable NMR spectra could be obtained in deuterated DMSO for **1** and **2**. Diamagnetism for **1** and **2** can be clearly seen from their respective well-resolved signals, whereas the paramagnetic **3** showed broadened signals with low intensity. The ^1H NMR spectra for the diamagnetic complexes were dominated by multiplets (7.51–7.29 ppm for **1** and 7.51–7.16 ppm for **2**) of triphenylphosphine which are upfield relative to the multiplets of the aromatic signals for the Schiff base chelators (see figure S1 for the ^1H NMR spectrum of H_2tdp). Confirmation of coordination is clearly observed by the disappearance of the broad uracil-amino group singlet (6.96 ppm for H_2tdp and 3.19 ppm for H_2sdp) and the appearance of sharp singlets (12.72 ppm for **1** and 12.67 ppm for **2**) downfield due to the deprotonated form of the uracil-amino group (see figure S2 for the ^1H NMR spectrum of **2**). Further evidence arises from the imino singlets which are at lower frequencies (for **1** the signal is part of a 7.71–7.62 multiplet and for **2** at 8.01 ppm), in comparison to the free

Schiff bases (for H_2tdp at 9.79 ppm and for H_2sdp at 10.08 ppm). Magnetic equivalence was observed for the *trans-axial* triphenylphosphine co-ligands from the ^{31}P NMR spectra of the diamagnetic complexes since only a single peak was found for both complexes, respectively.

IR spectra of all the complexes show the intense peaks of the *trans*-[Ru-$(PPh_3)_2$] unit found nearly at the same positions between 750 and 690 cm^{-1} [26] (see figures S3–S5). Consistent with the ^{1}H NMR spectral analyzes, coordination is also affirmed based upon shifts observed in IR spectra of **1** and **2** relative to their free Schiff bases. The imino stretching bands shift to higher frequencies (e.g. from 1611 cm^{-1} in H_2tdp to 1665 cm^{-1} in **1**) upon coordination. In addition, shifts were also observed for the intense bands of the tdp chelator in **1** as well as the ν(S–CH_3) in **2** relative to their respective free ligands. For **3** the disappearance of the Schiff base moiety (for H_3hdp at 1608 cm^{-1}) supports the fact that hydrolysis occurred. Furthermore, only one broad ν(N–H) stretching band was found for the diamagnetic complexes, opposed to the two ν(N–H) stretching bands for the paramagnetic complex**.**

The highly delocalized Schiff base chelators afford similarities between the UV/Vis spectra of free Schiff bases and **1** and **2** (see figures S6–S8). For example, a series of common intra-ligand electronic transitions was observed for all complexes between 280 and 410 nm. Broad Metal-to-Ligand Charge Transfer (MLCT) bands are found for all three complexes: at 507, 509 (for the d^6 **1** and **2**), and significantly red-shifted 690 nm for the d^4 **3**, respectively. These MLCT bands are typical of octahedral Ru(II/IV) complexes with aromatic chelating moieties [27, 28]. No d-d transitions are found for the diamagnetic complexes, which could be due to their low-spin d^6 electron configurations. The same trend was observed with the paramagnetic d^4 complex, which is most likely due to a larger energy band gap which does not favor electronic transitions.

As expected, ruthenium(II) complexes (**1** and **2**) exhibit ESR silent diamagnetic behavior due to their non-variable spin states (S = 0), but ruthenium(IV) complexes can exhibit both diamagnetic (S = 0) and paramagnetic (S = 1) spin states depending on the nature of the ligand. A broad singlet (g_{iso}-value = 2.0757) observed in the X-band spectrum of **3** unequivocally confirms the presence of the paramagnetic Ru(IV) center (figure 2). Similar to **3**, the one-electron electrochemically oxidized species (at 295 K) of [$Ru^{III}Q_3$] {Q = 3,5-di-*tert*-butyl-*o*-quinone} and [$Ru^{III}(Q_x)$] {Q_x = 4,6-di-*tert*-butyl-*N*-phenyl-*o*-iminobenzoquinone} afforded isotropic singlets with g_{iso} = 1.991 and 2.001, respectively [29].

3.2. *Electrochemistry*

Each complex showed a single redox couple which exhibited diffusion controlled behavior at increasing scan rate. For example, see figure S9 for the overlay voltammograms of **3** for scan rates ranging from 100 to 300 mV, at increments of 25 mV. Peak current ratios approaching one were observed for all complexes, implying that the redox couples are for one-electron redox processes. More interesting is that **1** has a smaller peak to peak separation (ΔE = 80 mV, refer to table S1) than ferrocene (ΔE = 90 mV), which indicates faster electron transfer kinetics. However, slow electron transfer kinetics were observed for **2** and **3** which indicate quasi-irreversibility with peak to peak separations of 110 and 100 mV, respectively (figure 1).

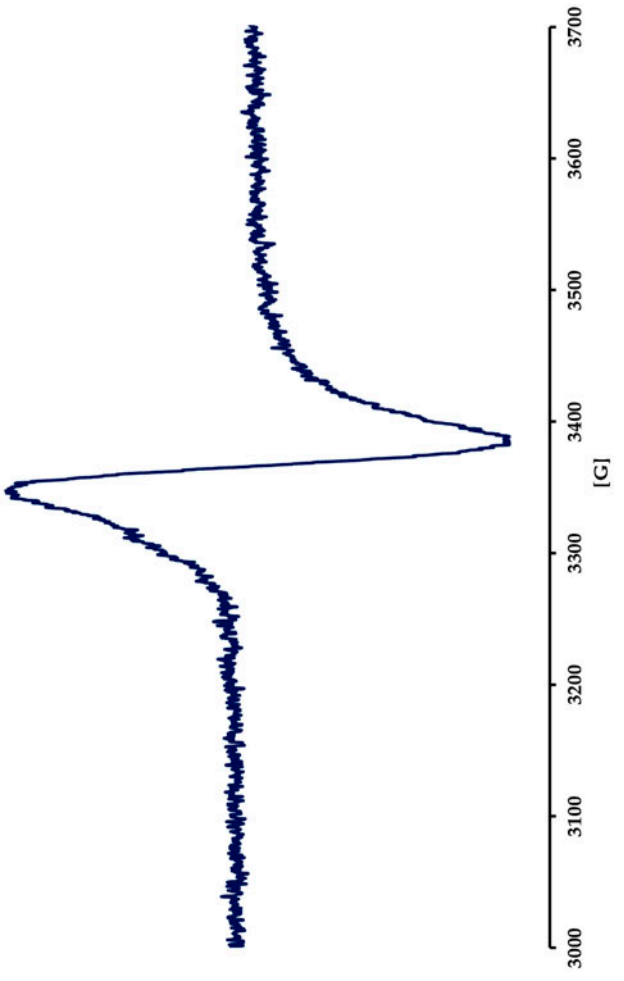

Figure 2. X-band EPR spectrum of **3** at 298 K. Instrument settings: microwave bridge frequency, 9.8 GHz; microwave bridge attenuator, 20 dB; modulation frequency, 100 kHz; modulation amplitude, 5 G; center field, 3500 G.

The redox couples of the complexes are ascribed to metal-based processes as they had similar half-wave potentials to other ruthenium complexes with Schiff base chelates. These literature trends show that for **1** and **2** the redox couple Ru(II/III) is observed, whereas for **3** it had similar half-wave potentials to ruthenium(III) compounds ascribed to the Ru(III/IV) redox couple. For example, in the case for the complexes, *trans*-[$Ru^{II}(^{R}L)(PPh_3)_2(CO)Cl$] {$H^{R}L$ = (2-benzylimino-methyl)-4-R-phenol, R=H, Cl, Br or OMe}, which displays quasi-reversible metal centered processes in DCM between 0.62 and 1.16 V ($E_{½}$ *versus* Ag|AgCl). The variable half-wave potentials are accounted to diverse electronic properties of *R*, where *R* with electron withdrawing character induce a higher oxidation potential and a reverse trend was found for electron donating *R* [30]. Paramagnetic ruthenium(III) compounds *trans*-[$Ru^{III}(L)(PPh_3)_2Cl$] in DCM showed comparable Ru(III/IV) redox couples (*versus* Ag|AgCl) [7].

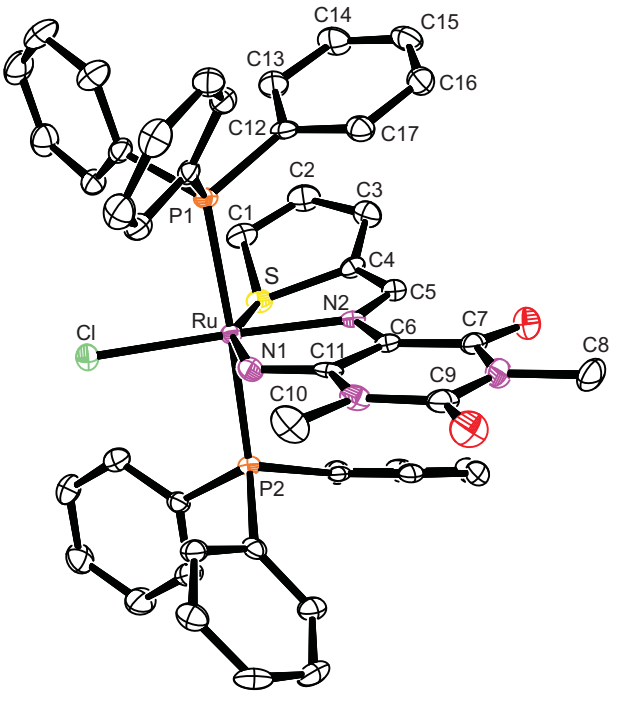

Figure 3. An ORTEP view of **1** showing 50% probability displacement ellipsoids and the atom labeling. Hydrogens were omitted for clarity.

3.3. *Crystal structure of 1*

The metal is at the center of a distorted octahedron with the basal plane defined by four donors, ClSN1N2, while the axial plane constitutes *trans* triphenylphosphines (figure 3). The distortion is enforced by the Htdp tridentate chelator (within the basal plane), which affords two constrained five-membered chelate rings [S–Ru–N2 = 80.9(7)° and N1–Ru–N2 = 78.8(1)°]. As a result, the equatorial bond angles [Cl–Ru–N2 = 167.66(7)° and S–Ru–N1 = 159.14(8)°] deviate considerably from linearity. Inevitably, the N1–Ru–N2 bite angle induces a wider C6–N2–C6 [123.5(3)°] bond angle than the ideal 120° for a bridging sp^2 hybridized nitrogen. However, the C(5)=N(2) bond distance of 1.313(4) Å is indicative of a Schiff base coordinated to ruthenium(II) [6, 29].

The metal amido [Ru–N1 = 2.036(3) Å] bond is shorter than the metal imino [Ru–N2 = 2.053(2) Å] bond as expected, with the latter comparable to ruthenium(II) complexes with Schiff base chelates [6, 29]. For example, a Ru–N_{imino} of 2.084(3) Å was observed for [Ru^{II}(L3)(CO)(PPh_3)] [10]. The nearly equidistance Ru–P bonds of **1** [Ru–P1 = 2.395(1) Å and Ru–P2 = 2.372(1) Å] forms a P1–Ru–P2 angle of 175.28(3)°.

Thiophene ligands exhibit diverse coordination modes ranging from η^1(S), η^1(C), η^2(C_2), η^4(C_4), and η^5(C_4S). A bond distance of 2.362(1) Å for the Ru–S bond is typical of η^1(S) coordination. The Ru–$S_{thienyl}$ bond was similar to [Ru(bpy)$_2$-*Y*-P,S](PF_6)$_2$, where for *Y* = PT_3 (3′-(diphenylphosphino)-2,2′-terthiophene) and *Y* = PMe_2T_3 (5′,5″-dimethyl-3′-(diphenylphosphino)-2,2′:5′2″-terthiophene) the bond distances were 2.346(1) and 2.362

(2) Å, respectively [31]. The sp^3 hybridized sulfur induces longer C–S [C1–S = 1.725(3) and C4–S = 1.749(3) Å] bond lengths within the thiophene ring, in comparison to delocalized C–S bonds found for uncoordinated thiophene rings. This implies that delocalization only occurs through the thiophene ring carbons, which is evident from the respective bond distances [C1–C2 = 1.353(4), C2–C3 = 1.426(4) and C3–C4 = 1.362(5) Å]. This was also observed for $[Ru^{II}(bpy)_2(dppe\text{-}terth\text{-}P,S)](PF_6)_2$ {bpy = 2,2′-bipyridyl, dppe-terth = 3′-(diphenylphosphino)-2,2′:5′2″-terthiophene] which had longer interthiophene ring C–S [1.744(3) and 1.751(3) Å] bond distances than its analogous compound, $[Ru^{II}(bpy)_2(dppe\text{-}terth\text{-}P,C)](PF_6)_2$,with C–S bond distances of 1.720(6) and 1.735(1) Å [32]. The thiophene moiety of **1** lies out of the basal plane by 31.14°, which could be induced either by the break in delocalization between the bridging C–S–C within the ring system or the pi-stacking [interplanar spacing = 3.696 Å] between the thiophene ring and the C12C17 phenyl ring of the triphenylphosphine co-ligand.

3.4. *Crystal structure of 3·CHCl$_3$*

Complex **3** co-crystallizes with a chloroform molecule in a triclinic unit cell (figure 4). Within the N1N2Cl1Cl2 basal plane, the small N1–Ru–N2 [78.0(1)°] bite angle causes the chlorides to be further apart resulting in a Cl1–Ru–Cl2 angle [97.64(2)°] deviating from the ideal 90° angle. This is not surprising as the geometrical parameters of the five-membered

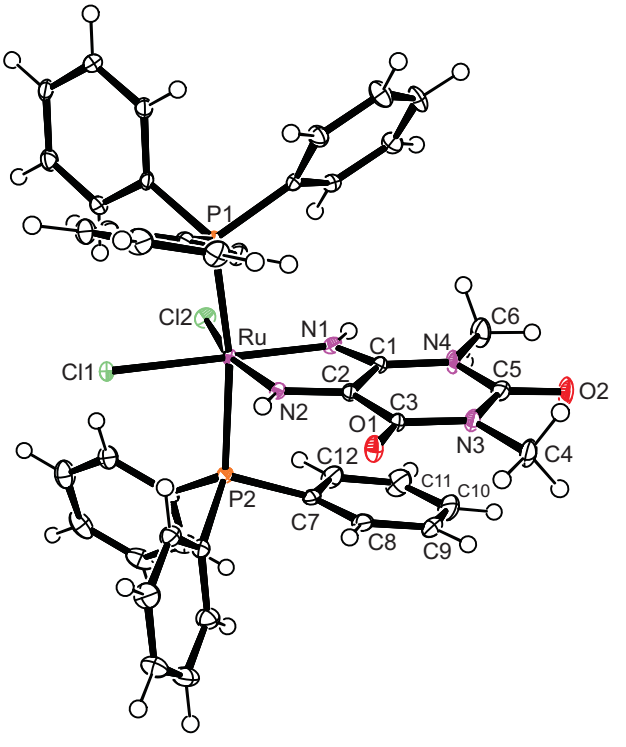

Figure 4. An ORTEP view of **3** showing 50% probability displacement ellipsoids and the atom labeling. The solvent of recrystallization has been omitted for clarity.

chelate ring of **3** were similar to those found in the chelate rings of ruthenium(II) bipyridine (bpy) complex, *cis*-[Ru(bpy)$_2$CO)(OH$_2$)] [33]. The constrained five-membered chelate ring resulted in a non-ideal octahedron where the basal plane *trans* [Cl1–Ru–N1 = 175.29(8)° and Cl2–Ru–N2 = 164.70(7)°] angles deviate from linearity. Although no difference in steric hindrance between **1** and **3** that influences *trans*-axial linearity is observed, a smaller angle was observed for **3** [P1–Ru–P2 = 170.34(2)°] relative to **1** [175.28(3)°]. This larger difference in linearity for **3** could be ascribed to a weak intermolecular interaction between almost co-planar ring systems (centroid to centroid distance = 3.950 Å) of ddd and the C7–C12 phenyl ring of the P2-triphenylphosphine. This might also account for the small differences in bond distances found for the Ru–P bonds [Ru–P1 = 2.3878(7) and Ru–P2 = 2.4006(7) Å] (also observed in **1**).

Noteworthy, the coordination sphere bond distances within the basal plane for **3** are shorter than in **1** due to stronger Lewis acid character of the ruthenium(IV). The metal amido bonds [Ru-N1 = 2.017(3) and Ru–N2 = 1.969(3) Å] are not equal, due to better electron withdrawing group next to N2, which causes a shorter metal amido bond. The *trans*-influence of the amido nitrogens on chlorides is different, with dissimilar metal to chloride bonds [Ru–Cl1 = 2.4218(7) and Ru–Cl2 = 2.4361(8) Å]. Several examples are found in literature of ruthenium(IV) compounds stabilized by amido donor chelates [34, 35]. Among these examples are [Ru^{IV}(bpy)(L–H)$_2$](PF$_6$)$_2$ and [Ru^{IV}(L–H$_2$)(L–H)$_2$](ZnCl) {L–H$_2$ = 2,3-diamino-2,3-dimethylbutane}, where a L–H moiety is a monoanionic bidentate chelator. These compounds were isolated from chemical oxidations via liquid bromine using the metal precursor, [Ru^{II}(bpy)(L–H$_2$)$_2$](X); X = PF$_6$ or ZnBr$_4$ [36].

4. Conclusion

Ruthenium(II/IV) complexes containing uracil were isolated. The crystal structure of **1** shows that Htdp is a mono-anionic tridentate chelator and the same coordination behavior was spectroscopically confirmed for the Hsdp in **2**. However, hydrolysis of the H$_3$hdp (into the dianionic bidentate ddd chelator) induced chemical oxidation which led to isolation of **3**. The presence of the Ru(IV) center was confirmed by ESR spectroscopy. These ruthenium complexes contain comparable geometrical parameters similar to ruthenium complexes found in literature, the classical equatorial coordination behavior of the chelators is enforced by the *trans*-[Ru(PPh$_3$)$_2$] core.

Supplementary material

CCDC 935218 and 935219 contains the supplementary crystallographic data for **1** and **3**·CH$_3$Cl. These data can be obtained free of charge at www.ccdc.cam.ac.uk/conts/retrieving.html, or from the Cambridge Crystallographic Data Center (CCDC), 12 Union Road, Cambridge CB2 1EZ, UK; Fax:+44(0)1223 336033; or Email: deposit@ccdc.cam.ac.uk]. Supplemental data for figures S1–S9 associated with this article can be found in the online version http://dx.doi.org/10.1080/00958972.2013.849808.

Acknowledgements

We are grateful to the University of KwaZulu-Natal and the National Research Foundation of South Africa for financial support.

References

[1] C. Ming Che, F. Siu. *Curr. Opin. Chem. Biol.*, **14**, 255 (2010).
[2] M.J. Clarke. *Coord. Chem. Rev.*, **232**, 69 (2002).
[3] C.L. Donnici, M.H. Araujo, H.S. Oliveira, D.R.M. Moreira, V.R.A. Pereira, M. de Assis Souza, M.C.A.B. de Castro, A.C.L. Leite. *Bioorg. Med. Chem.*, **17**, 5038 (2009).
[4] P. Krishnamoorthy, P. Sathyadevi, K. Deepa, N. Dharmaraj. *Spectrochim. Acta A*, **77**, 258 (2010).
[5] S. Kannan, R. Ramesh. *Polyhedron*, **25**, 3095 (2006).
[6] D.K. Seth, P. Gupta. *Polyhedron*, **31**, 167 (2012).
[7] R. Raveendran, S. Pal. *J. Organomet. Chem.*, **692**, 824 (2007).
[8] H. Ng, N. Lam, M. Yang, X. Yi, I.D. Williams, W. Leung. *Inorg. Chim. Acta*, **394**, 171 (2013).
[9] M. Vadori, S. Pacor, F. Vita, S. Zorzet, M. Cocchietto, G. Sava. *J. Inorg. Biochem.*, **118**, 21 (2013).
[10] S. Mandal, S. Mandal, D.K. Seth, B. Mukhopadhyay, P. Gupta. *Inorg. Chim. Acta*, **398**, 83 (2013).
[11] G.S. Khan, A. Shah, Z. Rehman, D. Barker. *J. Photochem. Photobiol., B*, **115**, 105 (2012).
[12] I.N. Booysen, M. Ismail, T.I.A. Gerber, M. Akerman, B. van Brecht. *S. Afr. J. Chem.*, **65**, 174 (2012).
[13] K. Potgieter, P. Mayer, T. Gerber, N. Yumata, E. Hosten, I. Booysen, R. Betz, M. Ismail, B. van Brecht. *Polyhedron*, **49**, 67 (2012).
[14] H. Hamidov, J.C. Jeffery, J.M. Lynam. *Chem. Commun.*, 1364, (2004).
[15] J.J. Fiol, A. García-Raso, F.M. Albertí, A. Tasada, M. Barceló-Oliver, A. Terrón, M.J. Prieto, V. Moreno, E. Molins. *Polyhedron*, **27**, 2851 (2008).
[16] B.T. Khan, K. Annapoorna. *Inorg. Chim. Acta*, **171**, 157 (1990).
[17] I. Booysen, I. Muhammed, A. Soares, T. Gerber, E. Hosten, R. Betz. *Acta Cryst.*, **E67**, o1592 (2011).
[18] Oxford Diffraction. *CrysAlis CCD and CrysAlis RED*, Oxford Diffraction, Yarnton (2008).
[19] R.H. Blessing. *Acta Cryst.*, **A51**, 33 (1995).
[20] Bruker APEX2. *SAINT and SADABS*, Bruker AXS, Madison, WI (2010).
[21] G.M. Sheldrick. *Acta Cryst.*, **A64**, 112 (2008).
[22] L.J. Farrugia. *J. Appl. Cryst.*, **45**, 849 (2012).
[23] O.V. Dolomanov, L.J. Bourhis, R.J. Gildea, J.A.K. Howard, H. Puschmann. *J. Appl. Cryst.*, **42**, 339 (2009).
[24] N. Gunasekaran, N. Remya, S. Radhakrishnan, R. Karvembu. *J. Coord. Chem.*, **64**, 491 (2011).
[25] K. Nagaraju, R. Raveendran, Satyanarayan Pal, Samudranil Pal. *Polyhedron*, **33**, 52 (2012).
[26] J.D.E.T. Wilton-Ely, M. Wang, S.J. Honarkhah, D.A. Tocher. *Inorg. Chim. Acta*, **358**, 3218 (2005).
[27] P. Govindaswamy, Y.A. Mozharivskyj, M.R. Kollipara. *Polyhedron*, **23**, 1567 (2004).
[28] C. Ho, C. Che, T. Lau. *J. Chem. Soc., Dalton Trans.*, 967 (1990).
[29] A.K. Das, R. Hübner, B. Sarkar, J. Fiedler, S. Záliš, G.K. Lahiric, W. Kaim. *Dalton Trans.*, 8913 (2012).
[30] R. Raveendran, S. Pal. *J. Organomet. Chem.*, **695**, 630 (2010).
[31] C. Moorlag, O. Clot, M.O. Wolf, B.O. Patrick. *Chem. Commun.*, 3028 (2002).
[32] C. Moorlag, M.O. Wolf, C. Bohne, B.O. Patrick. *J. Am. Chem. Soc.*, **127**, 6382 (2005).
[33] D. Oyama, K. Suzuki, T. Yamanaka, T. Takase. *J. Coord. Chem.*, **65**, 78 (2012).
[34] E. Gonzalez, P.J. Brothers, A. Ghosh. *J. Phys. Chem. B*, **114**, 15380 (2010).
[35] C. Che, W. Cheng, W. Leung, T.C.W. Mak. *J. Chem. Soc., Chem. Commun.*, 418 (1987).
[36] W. Chiu, S. Peng, C. Che. *Inorg. Chem.*, **35**, 3369 (1996).